

Volume 52		1 January 2013		ISSN 0278-4343	
		CONTINENTAL SHELF RESEARCH			
Editors: Michael Collins Southampton, UK Richard W. Sternberg Seattle, WA, USA					
V.G. Dvoretzky and A.G. Dvoretzky		1 Epiplankton in the Barents sea: Summer variations of mesozooplankton biomass, community structure and diversity			
C. Kuang, X. Liu, J. Gu, Y. Guo, S. Huang, S. Liu, W. Yu, J. Huang and B. Sun		12 Numerical prediction of medium-term tidal flat evolution in the Yangtze Estuary: Impacts of the Three Gorges project			
M.C. Murrell, R.S. Stanley, J.C. Lehrter and J.D. Hagy III		27 Plankton community respiration, net ecosystem metabolism, and oxygen dynamics on the Louisiana continental shelf: Implications for hypoxia			
M.-L. Timmermans and P. Winsor		39 Scales of horizontal density structure in the Chukchi Sea surface layer			
C. Reyes-Hernández and A. Valle-Levinson		46 Fortnightly variations of the lateral structure of flow and hydrography at the Chesapeake Bay entrance			
A. Lapeussière, C. Michel, M. Gosselin, M. Poulin, J. Martin and J.-É. Tremblay		62 Primary production and sinking export during fall in the Hudson Bay system, Canada			
P.S. Dalyander, B. Butman, C.R. Sherwood, R.P. Signell and J.L. Wilkin		73 Characterizing wave- and current- induced bottom shear stress: U.S. middle Atlantic continental shelf			
J. Delavenne, P. Marchal and S. Vaz		87 Defining a pelagic typology of the eastern English Channel			
Y. Chen, G.-P. Yang, G.-W. Wu, X.-C. Gao and Q.-Y. Xia		97 Concentration and characterization of dissolved organic matter in the surface microlayer and subsurface water of the Bohai Sea, China			
M.M. Baustian, N.N. Rabalais, W.L. Morrison and R.E. Turner		108 Microphytobenthos along the Louisiana continental shelf during mid-summer hypoxia			
P. Costa Goela, J. Icely, S. Cristina, A. Newton, G. Moore and C. Cordeiro		119 Specific absorption coefficient of phytoplankton off the Southwest coast of the Iberian Peninsula: A contribution to algorithm development for ocean colour remote sensing			
<i>Continued on outside back cover</i>					
www.elsevier.com/locate/csr					

This article appeared in a journal published by Elsevier. The attached copy is furnished to the author for internal non-commercial research and education use, including for instruction at the authors institution and sharing with colleagues.

Other uses, including reproduction and distribution, or selling or licensing copies, or posting to personal, institutional or third party websites are prohibited.

In most cases authors are permitted to post their version of the article (e.g. in Word or Tex form) to their personal website or institutional repository. Authors requiring further information regarding Elsevier's archiving and manuscript policies are encouraged to visit:

<http://www.elsevier.com/copyright>

Contents lists available at [SciVerse ScienceDirect](http://www.sciencedirect.com)

Continental Shelf Research

journal homepage: www.elsevier.com/locate/csr

Research papers

Scales of horizontal density structure in the Chukchi Sea surface layer

Mary-Louise Timmermans^{a,*}, Peter Winsor^b^a Department of Geology and Geophysics, Yale University, 210 Whitney Ave., New Haven, CT 06515, United States^b Institute of Marine Science, School of Fisheries and Ocean Sciences, University of Alaska, P.O. Box 755220, Fairbanks, AK 99775-7220, United States

ARTICLE INFO

Article history:

Received 8 June 2012

Received in revised form

25 September 2012

Accepted 29 October 2012

Available online 6 November 2012

Keywords:

Chukchi Sea

Submesoscales

Horizontal wavenumber spectra

ABSTRACT

Horizontal density structure in the surface Chukchi Sea (in ice-free conditions) is investigated through analysis of high-resolution CTD data from two glider surveys. Temperature and salinity fields in the summer/fall surface layer indicate that horizontal temperature, salinity and density variability extends down to $\mathcal{O}(1)$ km submesoscales. Horizontal temperature and salinity gradients in the surface layer are universally non-compensating, with salinity dominating the density variability. Spectral slopes of k^{-3} (k is horizontal wavenumber) of horizontal potential density variance in the surface layer were found over 0.5 to 20 km wavelengths, consistent with quasi-geostrophic turbulence scaling. The character of horizontal density structure in the surface Arctic Ocean differs from k^{-2} spectra commonly observed in the lower latitudes. The observed submesoscale fronts play a role in setting surface-layer properties by restratifying the surface layer, in opposition to forcing such as winds that vertically mix the surface ocean.

© 2012 Elsevier Ltd. All rights reserved.

1. Introduction

Dynamics of the Arctic Ocean surface layer are of key significance to the surface-ocean heat budget, biological productivity, and the influence of the ocean on sea ice. The surface layer is mixed by convection (e.g. during ice growth and subsequent brine rejection), and shear-driven mixing by the wind or when overlying sea ice moves relative to the ocean. Restratification of the surface-layer takes place upon warming and surface freshening by ice melt and river run-off. Of relevance to this study is that surface-layer properties are also influenced by horizontal density fronts, and instabilities (which grow to form surface-layer eddies) that develop at fronts in the surface layer (e.g. Boccaletti et al., 2007; Thomas et al., 2008). Here we examine these submesoscale ($\mathcal{O}(1)$ km horizontal scale) processes that are active in the weakly stratified ocean surface layer which is characterized by a relatively small Rossby deformation radius ($\mathcal{O}(1)$ km) (Thomas et al., 2008). The submesoscales provide a critical dynamical link by transferring energy and properties from the mesoscale ($\mathcal{O}(10)$ km horizontal scale) flow field to the very small-scale processes that influence dissipation and mixing in the Arctic Ocean.

Lateral restratification of the surface layer takes place when closely spaced vertical isopycnals (fronts) slump under gravity as more dense fluid flows under adjacent lighter waters. Rotation

limits the gravitational slumping leading to geostrophic balance. The result is a restratified surface layer with tilted isopycnals and light water over dense water. Observations confirm that submesoscale restratification is actively occurring in the mid-latitudes (e.g. Ferrari and Rudnick, 2000; Hosegood et al., 2006), and in the Arctic Ocean under sea ice (Timmermans et al., 2012). Lateral restratification, which opposes vertical mixing, influences the heat budget of the surface Arctic Ocean (since shallower layers, to which vertical turbulent mixing is confined, result in solar insolation being distributed over a thinner region) and can also influence biological productivity by affecting the depth that determines light levels available to phytoplankton for growth.

In the mid-latitude oceans, an indirect signature of submesoscale restratification is compensating lateral density gradients (i.e. horizontal temperature and salinity gradients in the surface layer that cancel in their effect on density) down to small lateral scales (e.g. Ferrari and Rudnick, 2000). Compensation arises when lateral restratification (by frontal slumping and surface-layer instabilities) is followed by vertical mixing. This destroys lateral density gradients, leaving behind only compensated temperature-salinity gradients. Compensated temperature and salinity gradients are more prevalent where mixing levels are higher. Rudnick and Martin (2002) found that compensation tends to increase with surface-layer depth. Beneath sea ice, the Arctic Ocean winter surface layer is almost always at the surface freezing temperature for seawater, and density compensation would not be observed regardless of the strength of vertical mixing (see Timmermans et al., 2012). Further, the coefficient of thermal expansion is very small at the cold temperatures of the Arctic Ocean (even in the

* Corresponding author.

E-mail addresses: mary-louise.timmermans@yale.edu (M.-L. Timmermans), pwinsor@alaska.edu (P. Winsor).

absence of sea ice) and variations in temperature can have very little effect on density. Nevertheless, Ice-Tethered Profiler measurements under sea ice reveal lateral density variability down to small lateral scales in the surface layer and surface-layer stratification that results from submesoscale lateral processes (Timmermans et al., 2012). Relatively fresh thin mixing layers (to which turbulent mixing is confined) at the top of the surface layer were associated with isopycnal slumping and dynamical restratification.

Horizontal wavenumber spectra are computed to examine how the potential density variance in the surface ocean is distributed among spatial scales. In the surface Arctic Ocean under sea ice, a k^{-3} scaling (horizontal wavenumber k) is found over 5–50 km wavelengths (Timmermans et al., 2012). This is steeper than in the subtropical North Pacific where spectra of horizontal surface-layer density or temperature have been found to scale as k^{-2} for scales between about $\mathcal{O}(10)$ km and $\mathcal{O}(100)$ km (e.g. Samelson and Paulson, 1988; Cole et al., 2010). Note that over smaller scales, between 1 km and 10 km, Samelson and Paulson (1988) found the temperature spectrum proportional to k^{-3} , while Ferrari and Rudnick (2000) showed temperature and salinity variance spectra scale as k^{-2} for 100 m to 100 km scales. In the Gulf Stream region, Wang et al. (2010) found a temperature spectral slope of k^{-3} over $\mathcal{O}(10-100)$ km. The k^{-3} spectra are in good agreement with quasi-geostrophic turbulence scaling (Charney, 1971), while the shallow k^{-2} spectra are more commonly observed in models (see Capet et al., 2008) and are consistent with the surface quasi-geostrophic theory (SQG) appropriate in regions close to boundaries (Blumen, 1978). It is important to keep in mind that spectral slopes of complicated spatial systems cannot necessarily be taken as assessments of the governing dynamics (see e.g. Armi and Flament, 1985).

Here we present an exploratory evaluation of horizontal density structure at submesoscales, $\mathcal{O}(1-10)$ km, in the surface layer of the ice-free Arctic Ocean through an analysis of glider measurements from the Chukchi Sea in summer/fall. To our knowledge, the glider data presented here are the first of their kind from this part of the Arctic Ocean: continuous, long-duration hydrographic sampling with a resolution of about 120 m in the horizontal (and $\lesssim 10$ min between samples) from an Autonomous Underwater Vehicle (AUV) that does not disturb the surface layer of the ocean. This is in contrast to more traditional ship-based sampling where the horizontal and temporal spacing between CTD stations typically exceeds several kilometers and hours and the impact of turbulent mixing in the surface layer caused by the ship precludes assessment of detailed surface-layer features. Note that, under sea-ice in the Arctic, Ice-Tethered Profilers (Krishfield et al., 2008; Toole et al., 2011) have contributed valuable measurements to our understanding of surface-layer variability on scales down to the order 1 km submesoscales. In the next section, we describe the glider observations. In Section 3, we examine the scales of horizontal variability in the surface layer, assess horizontal temperature and salinity variability, and present examples of surface fronts and restratification in the upper Chukchi Sea. Our results are summarized and discussed in Section 4.

2. Glider measurements and general hydrographic structure

Data analyzed here were collected by Slocum gliders (Webb et al., 2001; further details can be found at <http://www.webbsearch.com/slocumglider.aspx>). The Slocum glider is an AUV that profiles in a saw-tooth pattern using changes in its buoyancy. Gliders obtain GPS positions upon surfacing and navigate underwater by dead reckoning to a compass bearing. The systems were equipped with Sea-Bird Electronics (SBE) Glider Payload CTDs

(GPCTDs); CTD sample rates were nominally 0.5 Hz. Measurements are analyzed from two glider surveys in the Chukchi Sea (Fig. 1): an approximately 240 km survey (this refers to along-track distance) in September 2010 and an approximately 140 km transect in

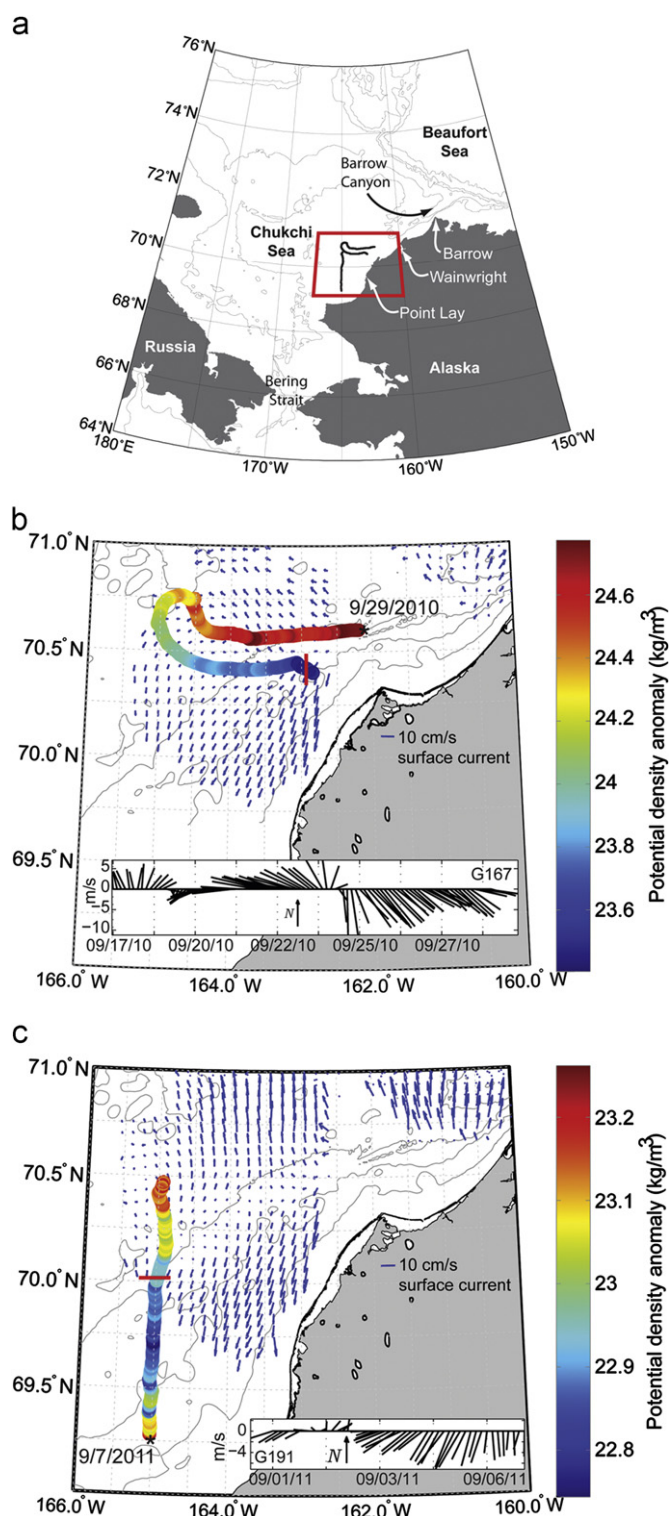


Fig. 1. (a) Map indicating the survey area and glider transects. Maps showing glider transects (b) G167 and (c) G191. End dates are shown for each transect; colors indicate potential density anomaly at 10 m depth; straight red lines mark the centers of the representative fronts plotted in Fig. 5; bathymetric contours are 20, 30, 40 and 50 m. Blue arrows indicate the mean surface currents during each survey and stick plots indicate winds for the duration of each survey (see text).

September 2011 (labeled G167 and G191, respectively, in Fig. 1b and c). Stronger current speeds associated with coastal jets limit operations close to shore, and surveys were carried out at least several tens of kilometers offshore where and when ambient flow speeds were small. The gliders profiled the water column in a saw-tooth pattern from around 3–5 m depth to the bottom at around 30–40 m depth, with forward glider velocities typically between 25 and 35 cm s⁻¹. The profiling pattern was such that at 10-m depth the interval between samples was around 120 m and 8 min.

The surveys were completed in open water conditions (with sea-surface temperatures about 10 °C above freezing) and no major water-mass fronts were crossed. Atmospheric conditions during both surveys were similar; wind data (NCEP North American Regional Reanalysis (NARR), Mesinger et al., 2006) taken from the center of each survey region indicate light to moderate winds of varying direction (Fig. 1b and c). During the open water seasons of 2010 and 2011, hourly surface currents were measured over the glider survey region in the northeast Chukchi Sea using

shore-based 5 MHz High-Frequency (HF) Radar systems, manufactured by CODAR Ocean Sensors (Statscewich et al., 2011). Field sites were located in the North Slope Borough of Alaska on native corporation lands in the villages of Barrow, Wainwright, and Point Lay (Fig. 1a). These locations allowed for data collection within 200 km of the coastline over an area of approximately 30,000 km². Current vectors were calculated at 6 km spatial resolution and represent velocity in the upper 1–2 m of the water column (Fig. 1b and c). Averages were taken over the periods September 17–29, 2010 (corresponding to survey G167) and September 1–7, 2011 (G191). Average surface currents within an area encompassing a few tens of kilometers from each glider track did not exceed 7 cm s⁻¹, with mean currents over the area approximately 3 cm s⁻¹ during each survey. Note that, the weak and variable currents in the survey region, combined with the 4–6 h intervals between glider surfacing (to obtain GPS positions), prevent estimation of reliable depth-averaged flow speeds based on glider drift from dead reckoning. However, in general, the small position discrepancies from dead reckoning are consistent with the weak

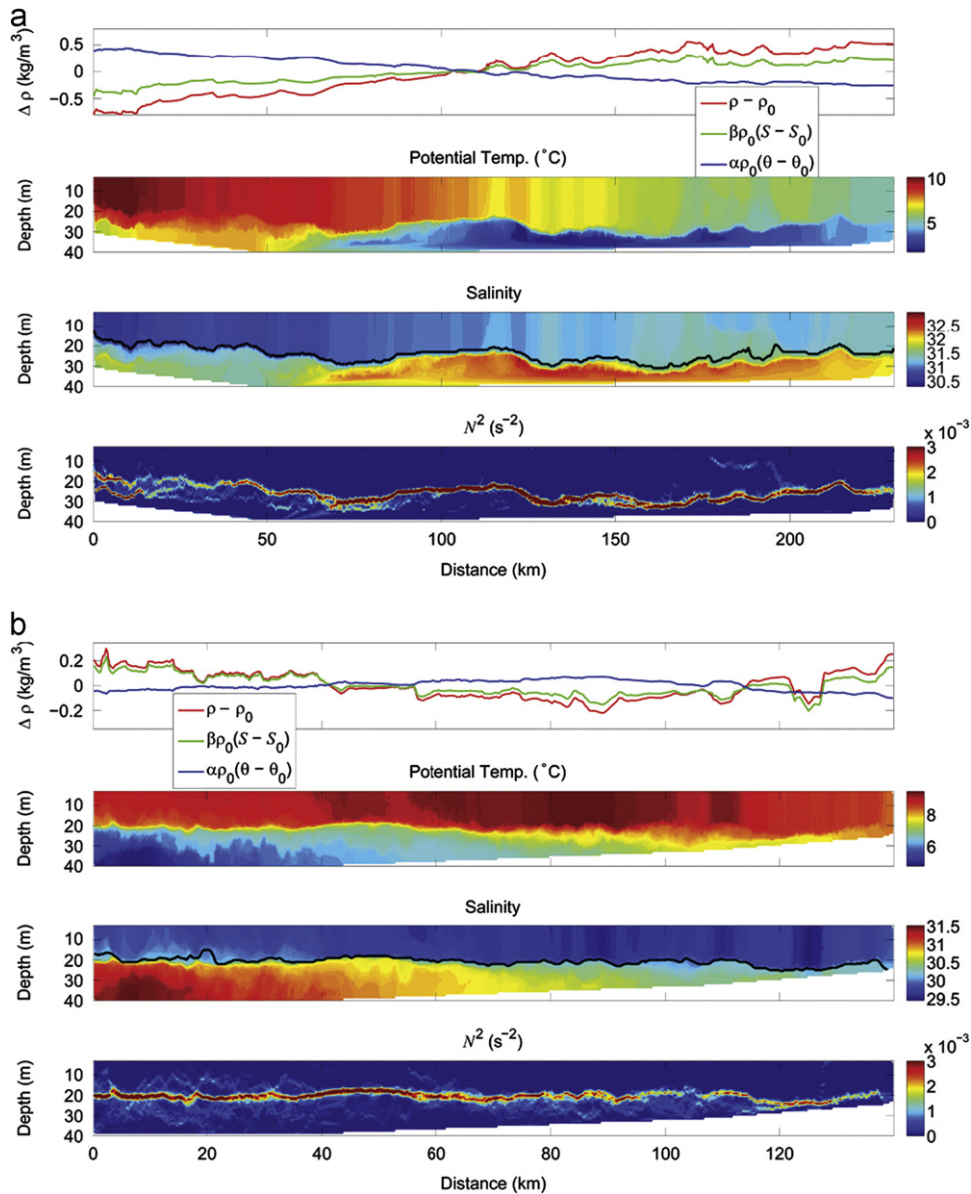


Fig. 2. Transects (a) G167 and (b) G191. Top panels: 10-m potential temperature (referenced to the surface) and salinity contributions to density perturbations, and the density perturbation. S_0 , θ_0 and ρ_0 are the mean values (at 10 m) for each section. Bottom panels: depth-distance sections of potential temperature, salinity and stratification. The black line in the salinity panel shows surface-layer depth computed using a critical density criterion of 0.25 kg m⁻³.

currents. We conclude that forward glider speeds ($25\text{--}35\text{ cm s}^{-1}$) were always larger than background currents during the surveys.

Glider CTD data processing followed Sea-Bird protocols for processing depth, salinity and temperature, including adjusting for thermal mass and spatial-temporal lag between the conductivity and the thermistor cells. Special attention was paid to the unpumped CTD data as the glider transited through strong stratification. Differences resulting from thermal mass and sampling issues were identified between up and downcasts (upward and downward flights). These mainly affect the limited depths of the strong pycnocline (thermocline/halocline), and display too warm waters, or alternatively too cold, when flying from cold to warm and vice versa, resulting in temperature and conductivity spikes. Using recent methodology (Garau et al., 2011) this effect was minimized by analyzing spatial-temporal structures of the full-resolution glider data, accounting for variable glider speed and sampling rates, to produce CTD data with minimal salinity and temperature spiking in the depth range of the pycnocline.

Generally, the shallow Chukchi Sea's water properties are established by the annual growth and melt cycles of sea ice, prevailing winds, and the transport of waters through Bering Strait. In summer and early fall, the Strait transport is northward on average and includes three major water masses (Coachman et al., 1975; Walsh et al., 1989); the cold, salty, nutrient-rich Anadyr Water, the warm, fresh, and nutrient-poor Alaskan Coastal Water (ACW), and Bering Shelf Water with intermediate properties, distinct from the Anadyr and Alaskan Coastal water masses. Coachman et al. (1975) maintain that Anadyr and Bering Shelf water masses mix to form Bering Sea Water (BSW) north of the Strait, whereas ACW maintains its properties on the Chukchi shelf. Chukchi bottom waters are modified by near-freezing, saline (dense) waters, which form in winter by freezing processes over both the Bering and Chukchi seas. In addition, cool, fresh surface waters, formed by ice melt, may be present. The ACW flows northeastward within the Alaskan Coastal Current toward the head of Barrow Canyon where it merges with waters carried eastward from the central shelf to form the canyon outflow. Therefore in summer and fall the eastern Chukchi shelf contains a complex of water masses that include ACW, meltwaters, dense winter waters, Bering Sea Water and mixtures of each (Weingartner et al., 2005; Pickart et al., 2005; Shroyer and Plueddemann, 2012).

The glider observations presented here indicated two prominent layers in the eastern Chukchi Sea south of Barrow Canyon: a relatively warm, fresh surface layer overlying a cooler, saltier layer (Fig. 2). The surface layer exhibited non-negligible vertical stratification across the layer at times as well as lateral density gradients in the layer. We define the base of the surface layer¹ by a critical density difference, taken to be 0.25 kg m^{-3} , from the shallowest measurement; this reliably selects the maximum vertical density gradient in the profiles (Fig. 2). The density gradient at the base of the surface layer is around 0.3 kg m^{-4} . Mean surface-layer depths are $26 \pm 4\text{ m}$ for G167 and $21 \pm 2\text{ m}$ for G191. In our analysis of horizontal density structure, we examine properties on a depth of 10 m, which is always well within the surface layer for both glider transects. The surface layer is not always entirely well mixed. An internal Rossby radius $L_R = NH/f$ (based on the density difference $\Delta\rho_H$ across the surface layer of depth H , where $N^2 \equiv -(g/\rho_0)(\Delta\rho_H/H)$, and $f \approx 1.37 \times 10^{-4}\text{ s}^{-1}$ is the Coriolis frequency) is the relevant lengthscale for submesoscale flows in the surface layer (Boccaletti et al., 2007; Hosegood et al., 2006). For both glider surveys, $L_R = 1.4 \pm 0.4\text{ km}$. This highlights the need for using AUV or towed vehicles for

observing the small scales of surface-layer submesoscale flows. Note that when vertical mixing is strong, the appropriate limiting lengthscale is $O(10)\text{ km}$, the Rossby radius based on the strong stratification across the surface layer base (see Ferrari and Rudnick, 2000; Hosegood et al., 2006). The weak stratification often exhibited by the surface layer appears to be a manifestation of lateral surface-layer restratification as will be shown in the next section.

3. Horizontal surface-layer structure

Glider measurements show horizontal density gradients at all observed scales in the surface layer (Fig. 2, top panel). Density at 10 m shows an approximately linear increase throughout the course of the G167 survey; density decreases for about the first half of the G191 survey, and then increases (Figs. 1 and 2). Superimposed on these largest scale gradients are mesoscale and submesoscale fluctuations, and possibly also temporal variability. Note that the gliders survey about 10 km horizontally in the surface layer in about 0.5 days or less. This sampling is faster than the evolution of both submesoscale features ($O(1)\text{ km}$ and $O(1)\text{ day}$) and mesoscale features ($O(10)\text{ km}$ and $O(10)\text{ days}$), and we assume that temporal variability does not interfere with our assessment of horizontal scales. Further, we do not expect advection of small-scale features by the mean flow to influence the representation of horizontal scales given that forward glider velocities are about 6–8 times faster than the mean currents in the surface layer.

Lateral gradients in potential temperature θ and salinity S in the surface layer are universally non-compensating and the measurements show that horizontal density gradients are not erased by vertical mixing in the Chukchi Sea, as they often are in the mid-latitudes. It is useful to introduce the horizontal density ratio $R_{\rho x} = \alpha\Delta\theta/\beta\Delta S$, where α and β are the coefficients of thermal expansion and saline contraction, respectively, and $\Delta\theta$ and ΔS are horizontal differences of potential temperature and salinity over a given distance. $R_{\rho x} = 1$ for complete compensation. In the mid-latitudes temperature typically dominates uncompensated density fronts and $R_{\rho x} > 1$ (see e.g. Hosegood et al., 2006). Salinity dominates density gradients for $|R_{\rho x}| < 1$. Note that lateral salinity fluctuations in the surface layer during the glider surveys here are typically $\lesssim 0.2$. These would be compensated by temperature changes $\lesssim 1^\circ\text{C}$ (for mean values of α and β), roughly the magnitude of fluctuations that are observed. Histograms of a horizontal Turner angle $Tu_x = \tan^{-1}(R_{\rho x})$ (Ferrari and Rudnick, 2000), for which complete horizontal density compensation occurs for $Tu_x = \pi/4$, show how lateral θ and S gradients measured here are non-compensating with salinity changes dominating density gradients, and a peak in the histogram around $Tu_x \approx 0$ (Fig. 3). Temperatures are well-above freezing, in contrast to the surface

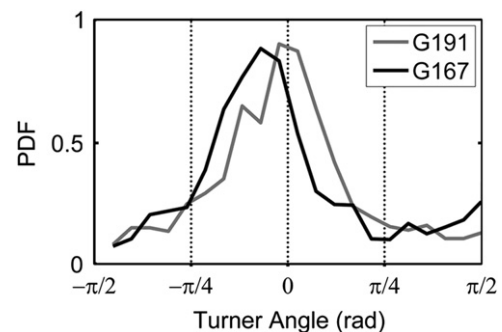


Fig. 3. PDF of Turner angle, $Tu_x = \tan^{-1}(R_{\rho x})$, at 10 m depth. The temperature and salinity differences were taken over 1 km (similar results are obtained differencing over 0.5–5 km).

¹ Note that we do not use the more common term “mixed-layer” in reference to the surface layer to avoid confusion when discussing its weak stratification.

layer under sea ice, for which the horizontal Turner angle is also zero. Note that lateral gradients in temperature have more influence on lateral gradients in density in the case of G167 (with a shift to the left of the peak in the PDF of Tu_x). For lengthscales between 0.5 and 5 km, the standard deviation of $\rho_0\beta\Delta S$ is about twice that

of $\rho_0\alpha\Delta\theta$ for G167, while for G191, the standard deviation of $\rho_0\beta\Delta S$ is about four times that of $\rho_0\alpha\Delta\theta$.

Wavenumber spectra are used to describe the horizontal potential density variance in the surface layer over wavelengths of 0.5–20 km. Spectra were computed by interpolating data at 10 m depth onto a 0.15 km grid in the horizontal (i.e. distance along the glider track). This is reasonable because glider sampling is faster than the evolution or advection of submesoscale or mesoscale features in this region of weak mean flow; furthermore, such features should have no preferred orientation in the horizontal plane. Spectra of horizontal potential density variance at 10 m were computed by removing a trend from the gridded data, and averaging the Fourier coefficients in wavenumber bands with more degrees of freedom at higher wavenumbers. Below the surface layer, vertical internal wave isopycnal displacements appeared to alias vertical gradients into small-scale horizontal structure here (see Rudnick and Cole, 2011). Further, the shallow survey region precluded analysis of sufficiently long deep sections that were well below the pycnocline. For glider mean speeds of 25 cm s^{-1} , and spacing between samples of 120 m and 8 min, the Nyquist wave number and frequency are 4.2 cycles per kilometer (cpkm) and 3.7 cycles per hour (cph). This frequency is higher than the surface layer buoyancy frequency ($\lesssim 2\text{ cph}$), the upper limit of the internal wave spectrum. We do not expect aliasing from internal waves at 10 m (see Rudnick and Cole, 2011).

The best-fit slopes for 10 m potential density variance over 0.5–20 km wavelengths are -2.8 ± 0.1 for both transects (Fig. 4). Spectral slopes are effectively k^{-3} . This differs from k^{-2} scaling that is more common (although not universal) in the mid-latitudes. The relatively steep horizontal wavenumber spectra found here are in agreement with the k^{-3} spectra found under sea ice in the central Canada Basin (Timmermans et al., 2012) and indicate less energetic small-scale structure than the k^{-2} scaling. While these -3 spectral slopes are consistent with quasi-geostrophic turbulence scaling, it remains an open question as to why they differ from some mid-latitude observational studies and model results. Spectral analysis is inadequate in many respects (Armi and Flament, 1985), and different submesoscale regimes in the surface layer of the ocean cannot be characterized with knowledge only of the spectral slope.

The glider data show evidence for restratification by slumping of submesoscale fronts, as shown in two representative segments from the glider transects (Fig. 5). The surface fronts have horizontal

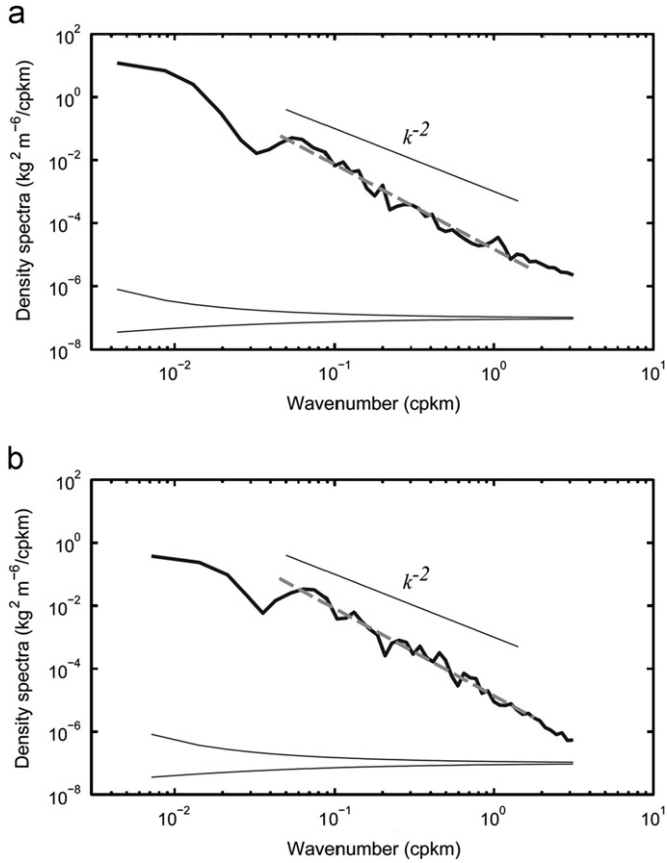


Fig. 4. Horizontal wavenumber spectra of potential density variance at 10 m depth in the surface from transects shown in Fig. 1 (a) G167 and (b) G191. The dashed lines are the best-fit slopes between 0.5 km and 20 km (-2.8 ± 0.1 in each case), effectively k^{-3} (-2 slopes are shown for reference). The 95% confidence intervals are shown. The number of degrees of freedom at each wavelength is taken to be twice the record length divided by the wavelength.

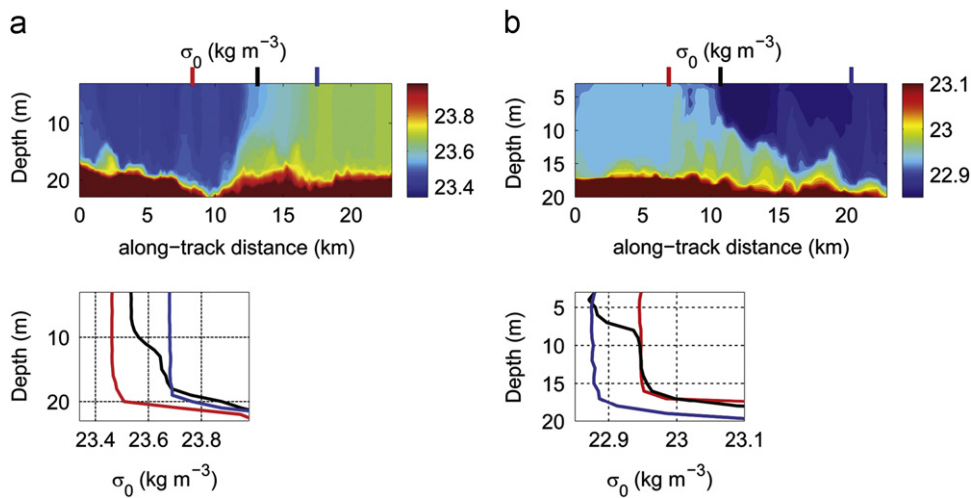


Fig. 5. Representative surface fronts from glider transects. Top panels show depth-distance sections of potential density (kg m^{-3}) anomaly (referenced to 0 dbar) with locations of the potential density profiles (bottom panel) marked. Profiles are centered at the front (black) and on either side of the front (red and blue). (a) East–west section from G167 on September 19, 2010 along 70.4°N with the front centered around 163°W . (b) South–north section from G191 on September 4, 2011 centered around 70°N .

density gradients of about $\partial\rho/\partial x \approx 0.03 \text{ kg m}^{-3}/\text{km}$, which is a lower bound given it is unlikely the glider transected exactly perpendicular to the fronts. Profiles at the fronts and on either side (Fig. 5, lower panels) suggest surface-layer restratification with shallow mixing layers at the top of the surface layer that are associated with lateral isopycnal slumping. At each front, we compute the balanced Richardson number, defined as $Ri \equiv f^2 N^2 / M^4$, where $M^2 \equiv -(g/\rho_0)\partial\rho/\partial x$. For Richardson numbers $\gtrsim 1$, surface fronts may be unstable to ageostrophic baroclinic instabilities (Stone, 1966; Molemaker et al., 2005); restratification by subsequent submesoscale eddies increases Ri (e.g. Boccaletti et al., 2007). Richardson numbers for the two representative fronts (Fig. 5) with $N \approx 0.007 \text{ s}^{-1}$ and $H \approx 20 \text{ m}$ are $Ri \approx 10$. These $Ri \gtrsim 1$ are consistent with the complicated structure around each of the representative fronts and frontal instabilities.

4. Summary and discussion

High spatial and temporal resolution glider measurements indicate lateral density variability over a range of scales and surface-layer stratification in the Chukchi Sea that is attributable to lateral processes. Slumping fronts are associated with shallow mixing layers at the top of the surface layer. Horizontal density variability at 10 m depth extends to scales $\mathcal{O}(1) \text{ km}$, consistent with the Rossby radius computed using the stratification within the surface layer. The spectral slope (k^{-3} scaling) of horizontal potential density variance is comparable with that found in the surface Canada Basin under sea ice, and steeper compared to the k^{-2} scaling that is often found in the mid-latitude ice-free oceans.

Future glider (or towed instrument) surveys, including surveys under sea ice, and high horizontal resolution measurements from buoys drifting in the sea-ice pack will reveal whether the k^{-3} scaling is universal in the surface Arctic Ocean. It is possible that the relatively weakly mixed, and shallow, surface layer of the Arctic Ocean behaves more like 2D quasi-geostrophic turbulence than the surface ocean in the mid-latitudes. Note that Ferrari and Rudnick (2000) find a k^{-2} potential density spectrum where the surface layer is between 100 and 150 m deep, much deeper than the case here. On the other hand, the study by Samelson and Paulson (1988), which indicated k^{-3} in the 1–10 km wavenumber band, was in a surface layer less than 70 m deep. Many more observations that resolve wavelengths less than 100 km are needed to examine the complex spatial variability in the surface Arctic Ocean, energy transfer to small scales and dissipation.

Key questions for future studies relate to comparing how surface-layer potential density variance is distributed over various lateral scales, and how lateral restratification influences surface-layer properties, in the presence of strong wind mixing in the Arctic Ocean. In this study, lateral density gradients at all measured scales suggest vertical mixing was not sufficiently strong during the glider surveys to lead to diffusion of density fronts. The data presented here were collected during moderate to weak atmospheric forcing; the surface layer exhibited weak stratification and no significant surface-layer depth changes. Note that the Chukchi Sea is often subject to strong surface forcing displaying large spatial gradients, which may cause local horizontal density variability. The weak vertical mixing inferred by the absence of horizontal density compensation suggests spatially variable surface forcing can be ruled out as the dominant mechanism for horizontal density variability.

Finally, it is worth noting that a parameterization for upper-ocean restratification by submesoscale, surface-layer eddies to represent fluxes between the upper ocean and the atmosphere or sea-ice cover has been formulated and implemented in coarse-resolution models (Fox-Kemper et al., 2008, 2011). Modification

to this implementation would be needed when surface-layer density variance spectra do not satisfy a k^{-2} scaling law, as found here and elsewhere in the Arctic Ocean under sea ice.

Acknowledgments

Funding was provided by the National Science Foundation Office of Polar Programs Arctic Sciences Section under award ARC-11076237. P.W. was funded by the Bureau of Ocean Energy Management, Shell Oil company and ConocoPhillips. We thank Hank Statscewich for field work and data analysis, Robert Shears for operating the vessel Tukpuk, and the village of Wainwright for their assistance.

References

- Armi, L., Flament, P., 1985. Cautionary remarks on the spectral interpretation of turbulent flows. *Journal of Geophysical Research* 90, 11,779–11,782.
- Blumen, W., 1978. Uniform potential vorticity flow: Part I. theory of wave interactions and two-dimensional turbulence. *Journal of the Atmospheric Science* 35, 774–783.
- Boccaletti, G., Ferrari, R., Fox-Kemper, B., 2007. Mixed layer instabilities and restratification. *Journal of Physical Oceanography* 37 (9), 2228–2250.
- Capet, X., McWilliams, J., Molemaker, M., Shchepetkin, A., 2008. Mesoscale to submesoscale transition in the California Current System. Part I: flow structure, eddy flux and observational tests. *Journal of Physical Oceanography* 38, 29–43.
- Charney, J., 1971. Geostrophic turbulence. *Journal of Atmospheric Science* 28, 1087–1095.
- Coachman, L., Aagaard, K., Tripp, R., 1975. Bering Strait: The Regional Physical Oceanography. University of Washington Press, Seattle, WA.
- Cole, S.T., Rudnick, D., Colosi, J., 2010. Seasonal evolution of upper-ocean horizontal structure and the remnant mixed layer. *Journal of Geophysical Research* 115 (C04012).
- Ferrari, R., Rudnick, D., 2000. Thermohaline variability in the upper ocean. *Journal of Geophysical Research* 105 (C7), 16,857–16,883.
- Fox-Kemper, B., Danabasoglu, G., Ferrari, R., Griffies, S., Hallberg, R., Holland, M., Maltrud, M., Peacock, S., Samuels, B., 2011. Parameterization of mixed layer eddies. III: implementation and impact in global ocean climate simulations. *Ocean Modelling* 39 (1–2), 61–78.
- Fox-Kemper, B., Ferrari, R., Hallberg, R., 2008. Parameterization of mixed layer eddies. Part I: theory and diagnosis. *Journal of Physical Oceanography* 38 (6), 1145–1165.
- Garau, B., Ruiz, S., Zhang, W., Pascual, A., Heslop, E., Kerfoot, J., Tintor, J., 2011. Thermal lag correction on Slocum CTD glider data. *Journal of Atmospheric and Oceanic Technology* 28, 1065–1071.
- Hosegood, P., Gregg, M.C., Alford, M.H., 2006. Sub-mesoscale lateral density structure in the oceanic surface mixed layer. *Geophysical Research Letters* 33.
- Krishfield, R., Toole, J., Proshutinsky, A., Timmermans, M.-L., 2008. Automated Ice-Tethered Profilers for seawater observations under pack ice in all seasons. *Journal of Atmospheric and Oceanic Technology* 25, 2091–2095.
- Mesinger, F., DiMego, G., Kalnay, E., Mitchell, K., Shafran, P., et al., 2006. North American regional reanalysis. *Bulletin of the American Meteorological Society* 87, 343–360.
- Molemaker, M.J., McWilliams, J.C., Yavneh, I., 2005. Baroclinic instability and loss of balance. *Journal of Physical Oceanography* 35 (9), 1505–1517.
- Pickart, R., Weingartner, T., Pratt, L., Zimmermann, S., Torres, D., 2005. Flow of winter-transformed Pacific water into the Western Arctic. *Deep-Sea Research II* 52, 3175–3198.
- Rudnick, D., Martin, J., 2002. On the horizontal density ratio in the upper ocean. *Dynamics of Atmospheres and Oceans* 36, 3–21.
- Rudnick, D.L., Cole, S.T., 2011. On sampling the ocean using underwater gliders. *Journal of Geophysical Research* 116.
- Samelson, R.M., Paulson, C., 1988. Towed thermistor chain observations of fronts in the subtropical North Pacific. *Journal of Geophysical Research* 93, 2237–2246.
- Shroyer, E.L., Plueddemann, A.J., 2012. Wind-driven modification of the Alaskan Coastal Current. *Journal of Geophysical Research* 117.
- Statscewich, H., Weingartner, T., Danielson, S., Grunau, B., Egan, G., Timm, J., 2011. A high-latitude modular autonomous power, control, and communication system for application to high-frequency surface current mapping radars. *Marine Technology Society Journal* 45 (3), 59–68.
- Stone, P., 1966. On non-geostrophic baroclinic stability. *Journal of Atmospheric Sciences* 23, 390–400.
- Thomas, L., Tandon, A., Mahadevan, A., 2008. Sub-mesoscale processes and dynamics. In: Hecht, M.W., Hasumi, H. (Eds.), *Ocean Modeling in an Eddy Regime*. Geophysical Monograph Series, vol. 177. American Geophysical Union, Washington, DC, pp. 17–38.

- Timmermans, M.-L., Cole, S., Toole, J., 2012. Horizontal density structure and restratification of the Arctic Ocean surface layer. *Journal of Physical Oceanography* 42, 659–668.
- Toole, J., Krishfield, R., Timmermans, M.-L., Proshutinsky, A., 2011. The Ice-Tethered Profiler: argo of the arctic. *Oceanography* 24 (3), 126–135.
- Walsh, J., McRoy, C., Coachman, L., Goering, J., et al., 1989. Carbon and nitrogen cycling within the Bering/Chukchi seas: source regions for organic matter affecting AOU demands of the Arctic Ocean. *Progress in Oceanography* 22, 277–359.
- Wang, D.-P., Flagg, C.N., Donohue, K., Rossby, H.T., 2010. Wavenumber spectrum in the Gulf Stream from shipboard ADCP observations and comparison with altimetry measurements. *Journal of Physical Oceanography* 40, 840–844.
- Webb, D., Simonetti, P., Jones, C., 2001. Slocum: an underwater glider propelled by environmental energy. *IEEE Journal of Oceanic Engineering* 26, 447–452.
- Weingartner, T., Aagaard, K., Woodgate, R., Danielson, S., Sasaki, Y., Cavalieri, D., 2005. Circulation on the north central Chukchi Sea shelf. *Deep Sea Research Part II: Topical Studies in Oceanography* 52 (24–26), 3150–3174.